EARTHQUAKE ENGINEERING AND STRUCTURAL DYNAMICS
Earthquake Engng. Struct. Dyn. **27**, 589–608 (1998)

RESPONSE OF INFILLED FRAMES USING PSEUDO-DYNAMIC EXPERIMENTATION

KHALID M. MOSALAM[1*†], RICHARD N. WHITE[2‡] AND GUSTAVO AYALA[3§]

[1] *Department of Civil and Environmental Engineering, University of California, Berkeley, CA 94720-1710, U.S.A.*
[2] *School of Civil and Environmental Engineering, Cornell University, Ithaca, N.Y. 14853, U.S.A.*
[3] *Institute of Engineering, National Autonomous University of Mexico, Mexico D.F. 04510, Mexico*

SUMMARY

An accurate and practical testing technique to study seismic performance of multi-storey infilled frames is formulated. This technique is based on the pseudo-dynamic method which can provide an acceptable approximation of the dynamic performance of structures under the influence of earthquake excitation. The pseudo-dynamic experimental technique is outlined and applied for testing a two-bay, two-storey gravity load designed steel frame infilled with unreinforced concrete block masonry walls. From the discussion of the results, the dynamic performance of the tested structure is assessed. © 1998 John Wiley & Sons, Ltd.

KEY WORDS: infill walls; pseudo-dynamic; experimental errors; energy distribution; equivalent truss

1. INTRODUCTION

Pseudo-dynamic experimentation is a testing procedure in which the dynamic response of the structure is calculated and the obtained displacements are statically applied to the structure in an *on-line* procedure. This technique is essentially identical to traditional time domain analysis but rather than idealizing the non-linear stiffness characteristics of the structure, the static restoring forces are directly measured from the specimen as the experiment proceeds. Computation of displacements is based on numerical integration of the governing second-order differential equations of motion of a system with assumed mass and damping properties and with a forcing function corresponding to a selected dynamic loading. During the test, actual displacements and restoring forces are measured using equipment normally used for static experiments. These measured quantitites are utilized in subsequent calculations. In this way, both dynamic effects and progressive damage of the specimen are included in the imposed displacements, and the procedure allows for an *in-depth* monitoring of the performance of the structure for the entire duration of *realistic* earthquake excitation.

Infilled frames have been investigated experimentally by many researchers, most often with monotonic (see e.g. Reference 1) or quasi-static cyclic loading (see e.g. Reference 2), and in a few cases with actual dynamic

* Correspondence to: Khalid M. Mosalam, Department of Civil and Environmental Engineering, University of California at Berkeley, Mail Code 1710, Berkeley, CA 94720-1710, U.S.A. E-mail: mosalam@ce.berkeley.edu
† Assistant Professor
‡ James A. Friend Family Professor of Engineering
§ Professor

Contract/grant sponsor: NCEER
Contract/grant sponsor: National Science Foundation
Contract/grant sponsor: State of New York

CCC 0098–8847/98/060589–20$17·50

Received 16 January 1997
Revised 8 July 1997

loading.[3] The present research is directed at providing additional experimental results for multi-bay, multi-storey infilled frames, utilizing pseudo-dynamic testing. Effect of openings is also investigated by introducing windows in some of the tested infill panels.

2. BACKGROUND

The pseudo-dynamic technique was first proposed in Japan about 25 years ago by Takanashi *et al.*[4] Since then, extensive pseudo-dynamic experimentation has been performed in Japan,[5] at the University of California, Berkeley,[6] and at the University of Michigan, Ann Arbor.[7] Results of the Berkeley and Michigan studies are summarized in Reference 8.

Different explicit and implicit numerical schemes are available to obtain a time-stepping approximate solution of the governing equations of motion. Although explicit methods may have stability problems, they predominate because of the iterations usually required with implicit methods. Several explicit methods have been examined by Shing and Mahin;[9,6] they recommend the use of a modified version of the Newmark algorithm which includes frequency-proportional numerical damping. Thewalt and Mahin[10] proposed a fully implicit hybrid solution technique where part of the solution is performed digitally and the remainder is solved in an analog form. Shing *et al.*[11] developed an unconditionally stable implicit time-integration algorithm which was successfully applied to test stiff reinforced masonry walls.[12]

The results from pseudo-dynamic experimentation can be very sensitive to measurement and control errors. This drawback led several researchers to focus on error analysis. The cumulative nature of experimental errors in pseudo-dynamic tests using explicit numerical integration algorithm was studied by Shing and Mahin.[13,14] The reliability of pseudo-dynamic testing was investigated by Yamazaki *et al.*[15] where experimental error behaviour is examined based on an elastic pseudo-dynamic test of a six-storey steel structure. Recently, Thewalt and Roman[16] presented several parameters for identifying errors and quantifying their magnitude and effect. For inelastic tests with either large systematic errors or small random errors, these parameters include: position error, cumulative over/undershooting, energy error, and input energy.

3. FORMULATION OF PSEUDO-DYNAMIC METHOD

The pseudo-dynamic method is implemented by idealizing the structure as a discrete-parameter system, formulating the equations of motion, and assuming the inertial and viscous damping characteristics. The structure is then loaded, and the displacements and structural restoring forces are *measured* during the experiment for subsequent use in the calculations. The governing differential equations of motion are numerically integrated using an *on-line* computer. The resulting computed displacement response, corresponding to a *specific* earthquake excitation, is then imposed on the tested structure by means of servo-hydraulic actuators.

The dynamic response of a general multi-degree-of-freedom structure is governed by

$$[M]\{a_{i+1}\} + [C]\{v_{i+1}\} + \{r_{i+1}\} = \{p_{i+1}\} \tag{1}$$

where $[M]$ and $[C]$ are the mass and damping matrices, respectively; $\{a_{i+1}\}$, $\{v_{i+1}\}$, $\{r_{i+1}\}$, and $\{p_{i+1}\}$ are, respectively, acceleration, velocity, restoring force, and external force vectors at the time $(i+1)\Delta t$ with time step Δt.

Stiff structures (e.g. frames with masonry infill walls) are best classified as short period structures. When the governing differential equations of motion of such structures are integrated using explicit numerical integration methods, stability problems may arise.[17] The recent trend in pseudo-dynamic experimentation is to use implicit methods, not only for their superior stability properties but also for their desirable spurious energy dissipation properties.[17]

The implicit Newmark algorithm developed by Hughes et al.[18] is utilized in the present study. In this algorithm the equations of motion (equation (1)) are satisfied in addition to the following difference relations:

$$\{d_{i+1}\} = \{d^{e}_{i+1}\} + (\Delta t)^2 \beta \{a_{i+1}\} \tag{2}$$

$$\{v_{i+1}\} = \{v^{e}_{i+1}\} + \Delta t\, \gamma \{a_{i+1}\} \tag{3}$$

where β and γ are parameters controlling stability and accuracy, respectively. The vectors $\{d^{e}_{i+1}\}$ and $\{v^{e}_{i+1}\}$ are the explicit parts of displacement and velocity, respectively, i.e.

$$\{d^{e}_{i+1}\} = \{d_i\} + \Delta t \{v_i\} + (\Delta t)^2 (0{\cdot}5 - \beta)\{a_i\} \tag{4}$$

$$\{v^{e}_{i+1}\} = \{v_i\} + \Delta t (1 - \gamma)\{a_i\} \tag{5}$$

An expression for $\{a_{i+1}\}$ can be obtained from equation (2). Upon substitution of this expression in equation (3) and then eliminating $\{v_{i+1}\}$ and $\{a_{i+1}\}$ from equation (1), the following *effective static problem* results:

$$[K^*]\{d_{i+1}\} = \{p^*_{i+1}\} \tag{6}$$

where

$$[K^*] = \frac{1}{(\Delta t)^2 \beta}[M] + \frac{\gamma}{\Delta t\, \beta}[C] \tag{7}$$

and

$$\{p^*_{i+1}\} = \{p_{i+1}\} - \{r_{i+1}\} + [K^*]\{d^{e}_{i+1}\} - [C]\{v^{e}_{i+1}\} \tag{8}$$

It should be noted that $\{r_{i+1}\}$ corresponds to the solution $\{d_{i+1}\}$ making the method an implicit one. The procedure, shown in Figure 1, is adopted in the present pseudo-dynamic experiments where the predictor phase is based on the *explicit* part of the displacement vector and the corresponding measured restoring force vector $\{r^{e}_{i+1}\}$. In general, the displacement vector $\{d_{i+1}\}$, obtained from the solution of the *effective static problem* given by equation (6), will differ from its explicit part $\{d^{e}_{i+1}\}$. Therefore, a residual force vector results; it is eliminated by iteration in the corrector phase shown in Figure 1. In general, this corrected phase should be applied until the error $\{d_{i+1} - d^{e}_{i+1}\}$ is eliminated. In the present implementation, a tolerance (TOL = 0·02 mm) is used to check this error quantity. This tolerance is taken as the smallest possible displacement increment which can be applied with the available hydraulic actuators. The reported results are based on applying only one iteration of the correction phase which was sufficient to satisfy the check shown in Figure 1. This was possible because of the use of a sufficiently small time step ($\Delta t = 0{\cdot}005$ sec) and a special ramping between displacement vectors $\{d_{i-1}\}$ and $\{d_i\}$ as illustrated in Figure 3. The numerical stability and accuracy of several numerical integration schemes, similar to the one adopted herein, have been analysed by Shing and Mahin.[6]

4. APPLICATION OF THE PSEUDO-DYNAMIC METHOD

The pseudo-dynamic algorithm shown in Figure 1 is used to test a quarter scale (i.e. the length scale factor $S_\ell = 4$), two-bay, two-storey steel frame infilled with unreinforced concrete block masonry (Figure 2). The specimen consisted of a semi-rigidly connected steel frame infilled with non-integral walls (i.e. without shear connectors between the frame members and the infills). The mechanical properties of the unreinforced masonry walls are summarized in Table I. As indicated in Figure 3, distinction is made between external transducers measuring the displacement vector of the structure $\{d_{\text{external}}\}$, used in the time-integration loop, and internal transducers measuring the displacement vector of the actuators $\{d_{\text{internal}}\}$, used to control the actuators in the servo-hydraulic loop.

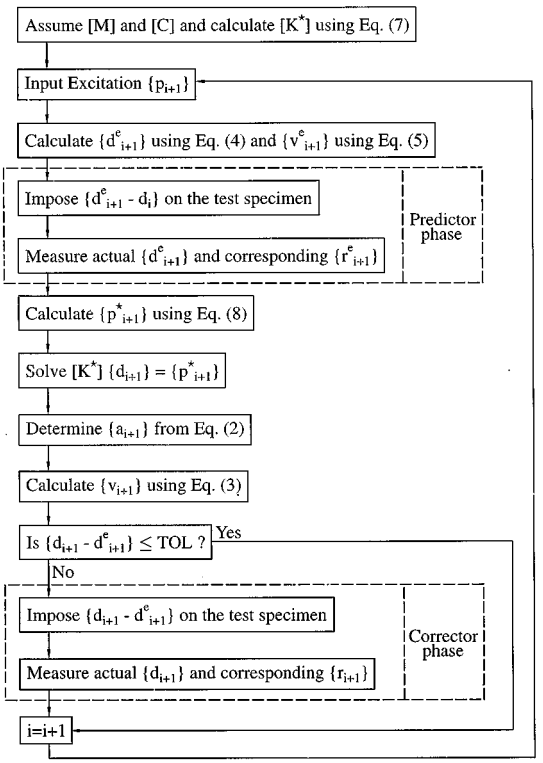

Figure 1. Pseudo-dynamic algorithm

4.1. *Ground motion*

Three earthquake records are selected as input ground motion. The first is the record at Taft-Lincoln School, S69E of the event at Kern County, California (21 July 1952). The second is the record at El-Centro, S00E of the event at Imperial Valley, California (18 May 1940). These two records represent, respectively, moderate and strong ground shaking typical of the North American west coast earthquakes. The third record is a late 1985 earthquake in the North Nahanni River area of the Northwest Territories of Canada. This record is an intra-plate type earthquake which is typical of the central and eastern regions of North America.

4.2. *Mass properties*

For the evaluation of the mass matrix, the prototype of the tested steel frame is assumed to be a part of a building with frame spacing of 16 ft (4877 mm) and carrying a 6 in (152 mm) thick reinforce concrete slab and design live load of 100 psf (4788 Pa). The resulting Prototype $[M_p]$ and corresponding model $[M_m]$ lumped mass matrices are

$$[M_p] = \begin{bmatrix} 35{\cdot}0 & 0{\cdot}0 \\ 0{\cdot}0 & 35{\cdot}0 \end{bmatrix} \quad \text{and} \quad [M_m] = \begin{bmatrix} 2{\cdot}2 & 0{\cdot}0 \\ 0{\cdot}0 & 2{\cdot}2 \end{bmatrix}, \text{ N sec}^2/\text{mm}$$

It should be noted that the mass in each storey accounts for the self-weight of the floor and 25 per cent of the design live load. Since the walls and the frame masses are much smaller than the floor mass, they are ignored. The model mass matrix is obtained by satisfying the similitude requirement,[19] namely, $[M_m] = [M_p]/S_\ell^2$.

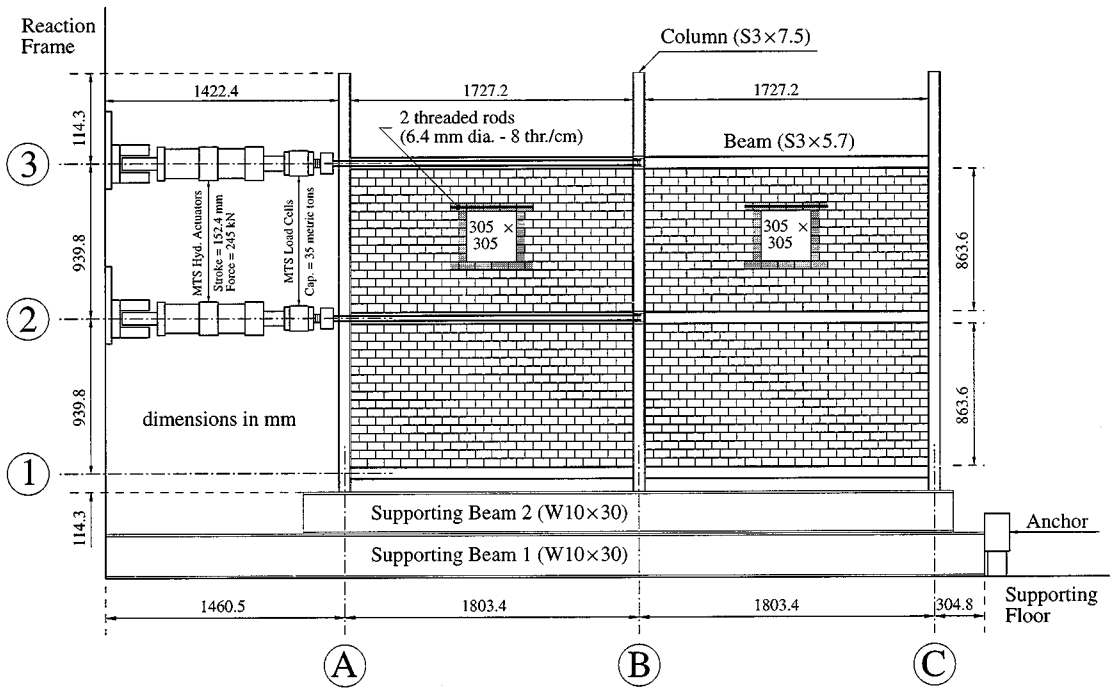

Figure 2. Layout of the tested specimen

Table I. Mechanical properties of unreinforced masonry components

$f_b^{\square}$ (MPa)	$f_{cyl}^{\triangle}$ (MPa)	f_b/f_{cyl}	$f_p^{\diamond}$ (MPa)	$E_p^{\diamond}$ (MPa)
27·6	21·4	1·29	22·8	10 300

□ block compressive strength based on net area
△ mortar cylinder compressive strength
◇ masonry prism strength (f_p) and stiffness (E_p) based on the face shell areas

4.3. *Stiffness properties*

Numerical and experimental studies of the infilled frame require estimation of the stiffness characteristics of the *undamaged* specimen. This estimation was achieved from preliminary experiments on the infilled frame using earthquakes with small Peak Ground Acceleration (PGA) (e.g. $0{\cdot}05g \leqslant \text{PGA} \leqslant 0{\cdot}15g$). These ground motions were sufficiently large to mobilize the composite action of the wall/frame system (i.e. provide sufficient lateral displacement to overcome the lack of fit between the wall and the frame) without any visible damage to the structure.

A sample result for the Taft earthquake scaled to PGA $= 0{\cdot}1g$ is illustrated in Figure 4(a), where a plot for the storey shear versus the inter-storey drift is shown for each storey. These plots are idealized in Figure 4(b) where non-linear elastic behaviour is assumed using the dashed line which follows the back-bone curve of the hysteresis loops. The back-bone curve shown in Figure 4(b) is approximated by the symmetric behaviour shown in Figure 4(c). This approximation is conducted by shifting the origin to the center of the flat region of

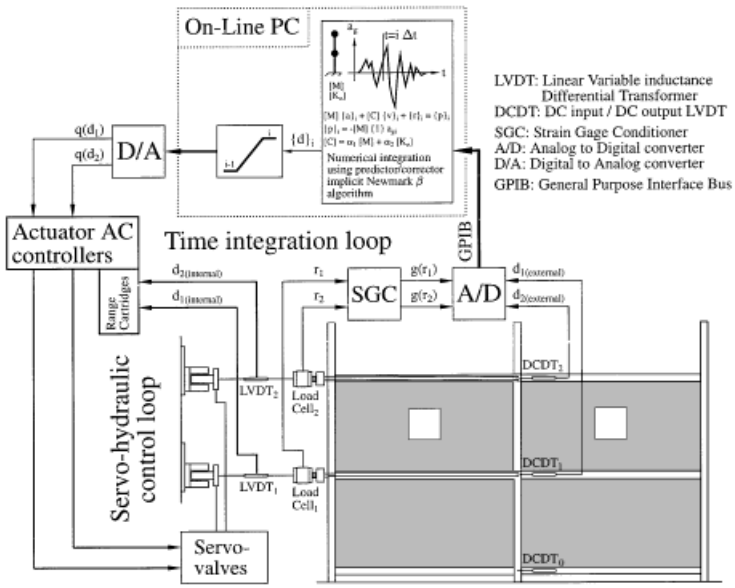

Figure 3. Schematic illustration of the pseudo-dynamic experiment

the plot and by taking the average of the stiffnesses in the positive and negative sides of the loop. The walls are assumed to be inactive during a displacement interval denoted by $2\Delta_{st}$, twice the storey *lack of fit* between the infill wall and the bounding frame. This lack of fit is thought to be caused mainly by *shrinkage* of the infill walls. From Figure 4(c), the two main tangent stiffness matrices can be identified as follows:

$$[K^{F}] = \begin{bmatrix} 4{\cdot}4 & -1{\cdot}4 \\ -1{\cdot}4 & 1{\cdot}4 \end{bmatrix} \quad \text{and} \quad [K^{IF}] = \begin{bmatrix} 65{\cdot}7 & -31{\cdot}0 \\ -31{\cdot}0 & 31{\cdot}0 \end{bmatrix}, \text{ kN/mm}$$

where $[K^{F}]$ and $[K^{IF}]$ are the linear stiffness matrices for the Frame and the Infilled Frame, respectively. These matrices are based on the assumption of rigid floors, i.e. *shear building* approximation. A transition zone exists between the situation of inactive walls, where the stiffness matrix is $[K^{F}]$, and that of walls in full contact with the bounding frame, where the stiffness matrix becomes $[K^{IF}]$. In this transition zone, the roughness along the interface between the walls and the frame members is degraded to provide the infilled frame composite action. From the assumed mass matrix $[M]$ and stiffness matrix (either $[K^{F}]$ or $[K^{IF}]$), the eigenproblem can be solved to obtain the eigensolution (frequency, f, and mode shape, $\{\Phi\}$) given in Table II.

4.4. Damping properties

Idealization of damping properties is probably the most uncertain step in structural dynamics. Several sources of material damping exist which makes its accurate idealization extremely difficult. In the present study, the simplest form of damping, namely *proportional damping*, is assumed, with the damping matrix $[C]$ given by

$$[C] = \alpha_1[M] + \alpha_2[K] \tag{9}$$

Following standard procedure (see e.g. References 20), the parameters α_1 and α_2 can be determined according to specified damping ratios in two modes. The second term in equation (9) may be based on $[K^{F}]$ or $[K^{IF}]$.

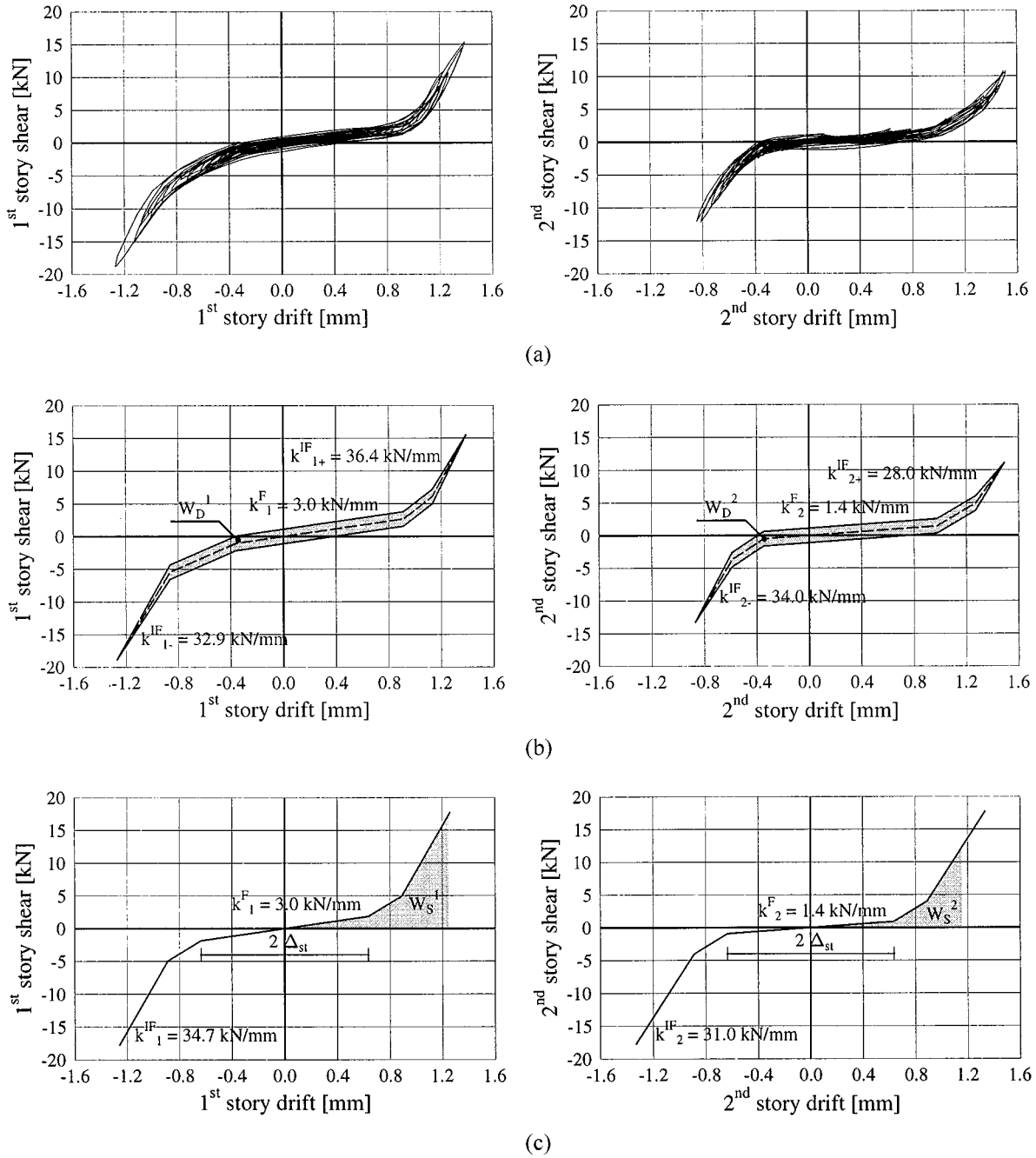

Figure 4. Stiffness properties; (a) Storey shear versus inter-storey drift due to Taft ground motion PGA = 0·1*g*; (b) Idealized hysteretic relations; (c) Idealized symmetric back-bone relations

The use of $[K^{F}]$ was selected in the present study because using $[K^{IF}]$ will lead to an over-estimation of $[C]$ before the walls come in full contact with the bounding frame. On the other hand, it is expected that damping due to hysteresis, produced by sliding between the walls and the frame members, is more important than the

Table II. Eigensolution for bare frame and infilled frame (subscripts 1 and 2 refer to first and second modes, respectively; superscript T denotes transpose)

	f_1 (Hz)	f_2 (Hz)	$\{\Phi_1\}$	$\{\Phi_2\}$
Frame (F)	3·15	7·59	$\{1{\cdot}00 \quad 2{\cdot}42\}^T$	$\{1{\cdot}00 \quad -0{\cdot}41\}^T$
Infilled Frame (IF)	12·14	31·24	$\{1{\cdot}00 \quad 1{\cdot}68\}^T$	$\{1{\cdot}00 \quad -0{\cdot}60\}^T$

viscous damping (refer to Section 4.6). For the bolted steel frame used in the present study, 2 per cent damping in the two modes of the bare frame is assumed. For these ratios, one obtains the following damping matrix $[C]$:

$$[C] = \begin{bmatrix} 3{\cdot}85 & -0{\cdot}88 \\ -0{\cdot}88 & 2{\cdot}10 \end{bmatrix}, \text{ N sec/mm}$$

4.5. Experimental errors

Experimental errors are inevitable; they are considered acceptable as long as their relative magnitudes, compared with the measured quantities, are 'reasonably small'. In the pseudo-dynamic procedure, experimental feedback is adopted in the step-by-step numerical integration. Therefore, errors introduced in any step are carried over to the subsequent computations, leading to potentially serious cumulative effects. Consequently, the actual displacement and force feedback values are likely to deviate from the originally computed and expected quantities.

Figure 5 shows a sample comparison of the calculated (using the pseudo-dynamic algorithm) and measured (during the pseudo-dynamic experiment) displacements for the two-bay, two-storey infilled frame under the Nahanni earthquake scaled to $0{\cdot}05g$ with assumed zero viscous damping. From this comparison, it may be concluded that the proposed pseudo-dynamic experimentation technique is reliable as far as experimental error propagation is concerned.

4.6. Numerical verification

The tested infilled frame shows a large change of stiffness due to the activation of the walls beyond the range of displacement needed to overcome the lack of fit between the walls and the bounding frame members. Accordingly, in the elastic stage, the structure is behaving as a *hard spring* which may lead to instability of the numerical integration. The standard time-domain analysis of a simple model (two degrees of freedom with lumped masses) of the tested structure with the idealized behaviour given in Figure 4(c) is performed. The *equivalent viscous damping ratio* (ξ^e) is given by

$$\xi^e = \frac{W_D}{4\pi W_S} \tag{10}$$

is considered to account for the hysteretic energy dissipation. As indicated in Figures 4(b) and 4(c), W_D is the area of the hysteresis loop (the amount of energy absorbed during one loading cycle) whereas W_S is the area under the back-bone curve (the amount of input energy at one loading cycle). It should be noted that both W_D and W_S are calculated at the same force level. Applying equation (10) at the maximum force level under the Taft earthquake scaled to $0{\cdot}1g$, the equivalent viscous damping coefficients (percentage of critical damping) obtained for the first and second storeys are 10·5 and 12·2 per cent, respectively. Based on the ratio between the energy absorbed in both storeys and the total input energy, ξ^e for the whole structure is determined to be 11·2 per cent.

A comparison of the numerically determined time histories of both the first and second floor displacements obtained with the simple model (using 11·2 per cent as equivalent viscous damping coefficients in both

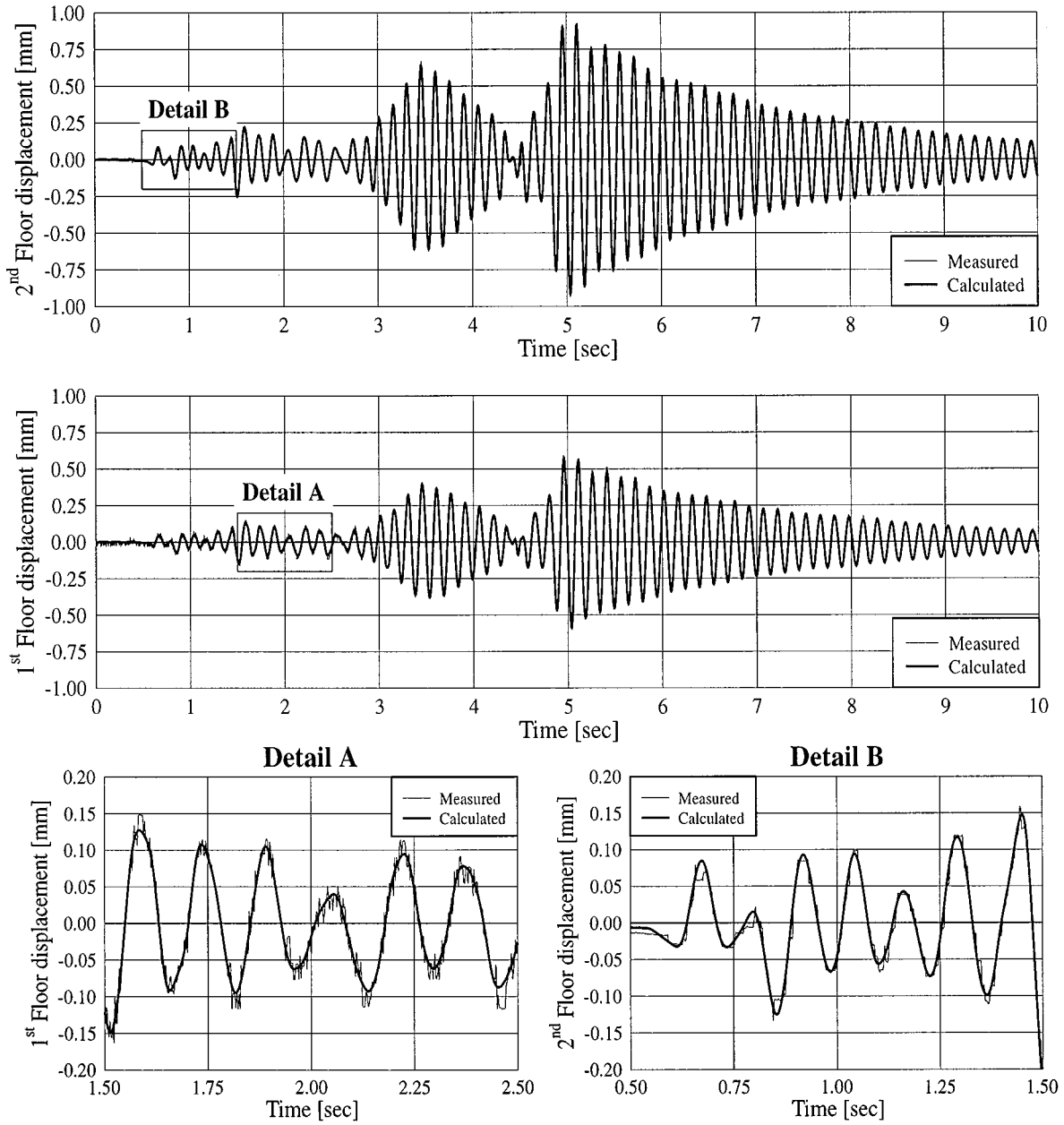

Figure 5. Comparison between measured and calculated displacements under 0·05*g* Nahanni earthquake

modes), and those obtained pseudo-dynamically (assuming zero viscous damping in the pseudo-dynamic experiment) is shown in Figure 6. Since non-zero viscous damping ratios may hide some numerical instabilities, if any are present, it was decided to use zero viscous damping ratios in the pseudo-dynamic experiment for the present case only, i.e. to check the stability and accuracy of the implementation of the pseudo-dynamic algorithm.

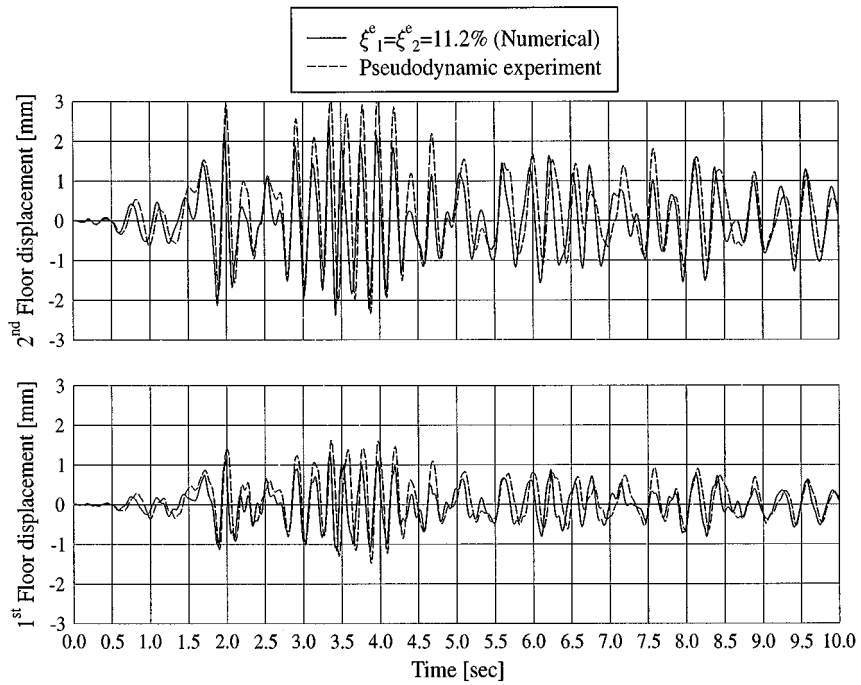

Figure 6. Time histories of displacements for Taft earthquake scaled to 0·1g

Figure 6 shows good agreement between the numerical results and the results from the pseudo-dynamic experiment. It is clear that the symmetry of the assumed structural behaviour (refer to Figure 4(c)) led to overestimation of the displacement in one direction (the negative direction) and underestimation of the displacement in the opposite direction.

4.7. Testing sequence

From the elastic response spectra of the selected three earthquake records (scaled to 1·0g), for the same PGA level, the Taft record produced the largest spectral responses. Therefore, it was chosen as the record to be used once the structure was damaged. The records were scaled on the basis of peak ground acceleration. Before any visible cracking in the masonry walls, the structure was subjected to Taft followed by El-Centro and finally Nahanni earthquake records. Once cracking occurred at Taft scaled to 0·2g, the structure was subjected to Taft only. In subsequent tests, the Taft record was incremented by 0·025g up to PGA = 0·4g. After this, a larger increment of 0·05g was considered up to PGA = 0·6g. Finally, the applied PGA was increased in 0·1g increments until PGA = 0·8g.

Although the initial state of the structure changed from the application of one record to the other because of the damage accumulation, it is thought that important information regarding structural modelling of degrading infill walls may be obtained from the selected experimental sequence. This is attributed to the fact that the idealization of infill walls and their interaction with the bounding frame members evolve with the level of damage in the walls. It should be noted that the low-level earthquakes ($<0·2g$ of Taft earthquake) produced no apparent damage in the tested structure. These records were applied to check the implementation of the pseudo-dynamic procedure and to correct for any problems arising during this preliminary stage.

5. RESULTS OF THE PSEUDO-DYNAMIC EXPERIMENT

The description of the obtained experimental results are discussed in this section. Crack patterns are presented along with a global response measure given by the corresponding storey-shear/inter-storey drift hysteretic relations. Another global measure of the structural performance, the distribution of the different energy terms, is also presented. On the local level, the straining actions in the frame members are evaluated using the measurements from strain gages at different sections of the frame members. Finally, comments are given on possible idealization of the infill walls using the so-called dual truss system.

5.1. Crack patterns and hysteretic relations

Cracking in masonry infills started at the second storey where cracks initiated close to the corners of the window openings. The existence of reinforced masonry bond beams on the top of the windows (see Figure 2) moved the cracks slightly away from the corners of the window openings. Because larger inter-storey drifts occurred in the first storey than the second, cracking in the second storey was temporarily arrested while more severe cracking occurred in the first storey. Sample results are shown in Figures 7–9 corresponding, respectively, to 0·2g, 0·4g and 0·6g PGA levels of the Taft earthquake. General observations on the cracking process in masonry infills are as follows:

(1) Cracks primarily occur along the interface between the horizontal (bed) mortar joints and the adjacent concrete blocks.
(2) Adjacent horizontal cracks become connected with cracks occurring along the mortar vertical (head) joints.
(3) The general form of cracking is a stepped diagonal pattern along the mortar bed and head joints connecting the two opposite loaded corners of the infill panel.

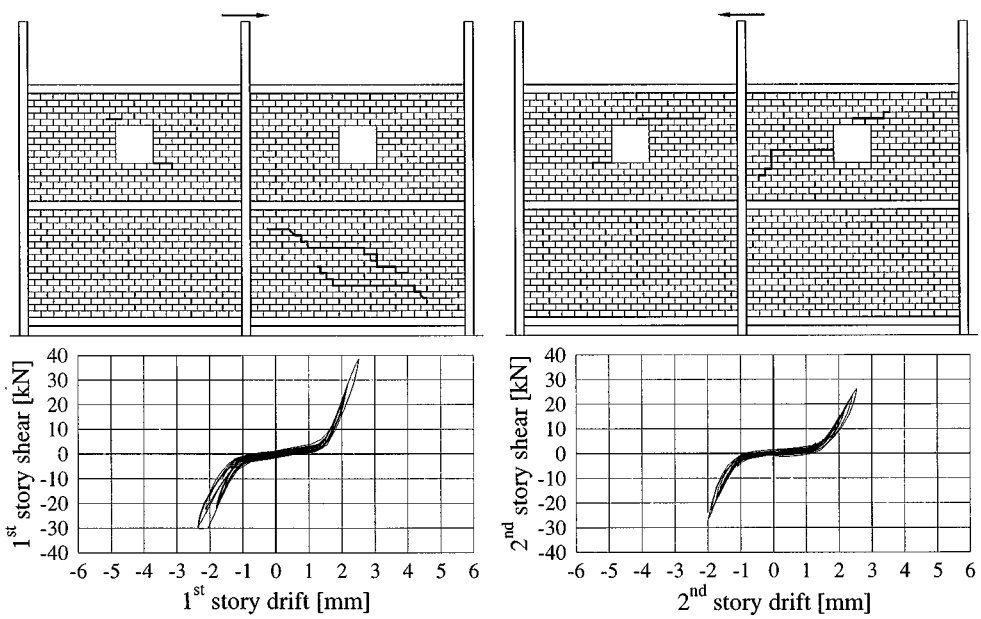

Figure 7. Crack patterns and hysteretic relations under Taft earthquake scaled to 0·2g

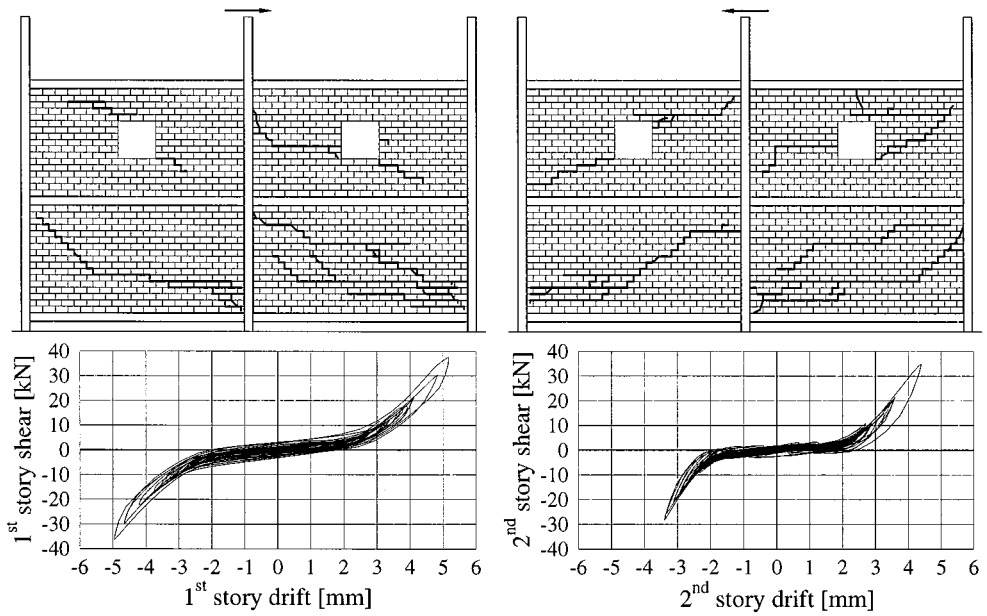

Figure 8. Crack patterns and hysteretic relations under Taft earthquake scaled to 0·4*g*

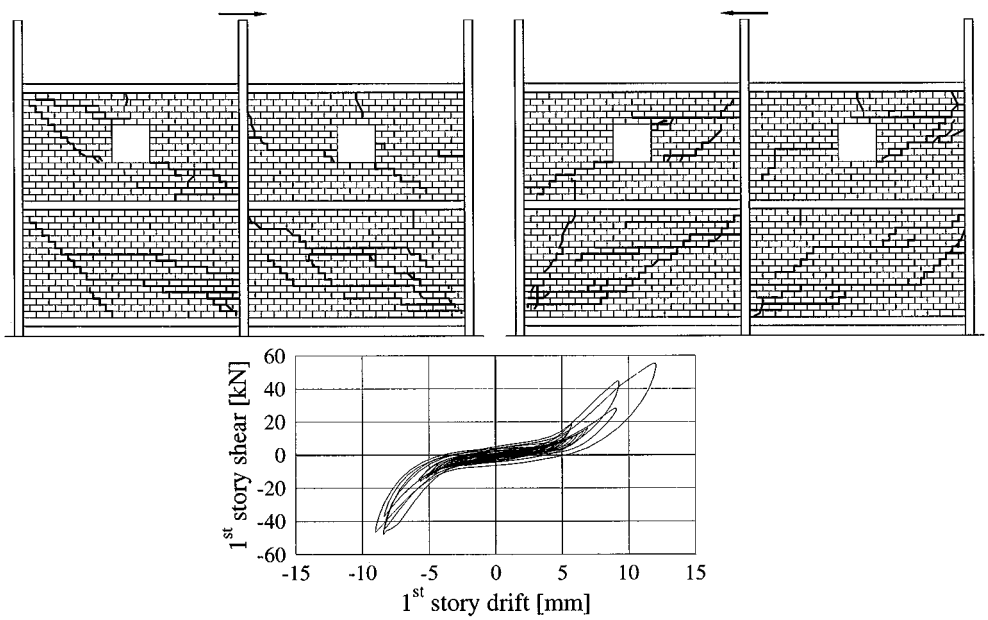

Figure 9. Crack patterns and hysteretic relation under Taft earthquake scaled to 0·6*g*

(4) Upon load reversal, complete closure of the cracks opposite to the loading direction is attained with new cracks initiating (or existing cracks opening) along the current loaded diagonal.
(5) Cracks tend to follow the weakest path in the panel. Therefore, upon repeated cyclic loading, most vertical cracks appeared in the mortar head joints rather than in the masonry blocks.
(6) Crack initiation is always accompanied by a large amount of energy released through hysteresis.

It is worth mentioning that the above observations are in agreement with those obtained from quasi-static testing of single-storey structures[21] similar to the two-storey structure presented here.

5.2. Energy distribution

When a structure is subjected to ground motion, energy (E_I) is *imparted* to it. During the dynamic loading, part of the absorbed energy is *temporarily stored* in the form of *kinetic* energy (E_K) and *strain* energy (E_S), and the rest is *dissipated* in the form of *damping* energy (E_D) and *hysteretic* energy (E_H).[22] Summarizing,

$$E_I = E_K + E_S + E_D + E_H. \tag{11}$$

Energy terms are calculated by procedures given in Reference 22 and 23 yielding values for E_I, E_K, E_D, and ($E_S + E_H$). To be able to determine a separate expression for the hysteretic energy, E_H, it is necessary to determine the area of the hysteresis loops[¶] obtained from the storey shear/inter-storey drift relationships. This may be achieved using the following expression in terms of the storey drift (D_i) and storey shear (S_i) of the ith storey,

$$E_H = \sum_{i=1}^{n} \int_{D_{\max}^-}^{D_{\max}^+} [S_i^{\text{upper}} - S_i^{\text{lower}}] \, dD_i \tag{12}$$

Superscripts (upper) and (lower) refer to the upper and lower curves of the hysteresis loop, respectively. Knowing the measured vectors of displacement $\{d\}$ and resulting force $\{r\}$, the storey quantities are defined as follows:

$$D_i = d_i - d_{i-1} \tag{13}$$

$$S_i = \sum_{k=i}^{n} r_k \tag{14}$$

where d_i and r_i are the displacement and restoring force of the ith floor, respectively.

Figure 10 shows the time histories of the imparted energies obtained from the pseudo-dynamic experiments using Taft, El-Centro and Nahanni earthquakes. In this plot, the PGA is scaled to 0·075g and 0 per cent viscous damping ratio is assumed in the pseudo-dynamic experiments for that level of PGA. It is noticed that the evolution of the imparted energy closely follows the distribution of the significant peaks of the ground motion. From the imparted energy of the Nahanni earthquake, it is obvious that this record will not produce any significant damage to the tested structure.

For the three levels of Taft earthquake and the corresponding crack patterns shown in Figures 7–9, the corresponding time histories for the energy terms are given in Figures 11(a)–11(c), respectively. The variations of the maximum values of the energy terms (E_I, E_H, and $E_{DH} = E_D + E_H$) versus the intensity of the ground motion given by its PGA are illustrated in Figure 12. These maximum values are obtained at the end of the applied records. It is obvious that the increase of the hysteretic energy (and consequently the dissipated energy E_{DH}) with increasing PGA becomes rapid at the onset of damage (i.e. at PGA = 0·2g). A similar trend is obtained for the imparted energy. For the infilled frame with cracked walls, the rate of increase of the

[¶] Under general loading (e.g. earthquakes), the calculation of the hysteretic energy should be carefully implemented because small loading/unloading cycles without complete load reversals may exist which require special attention.

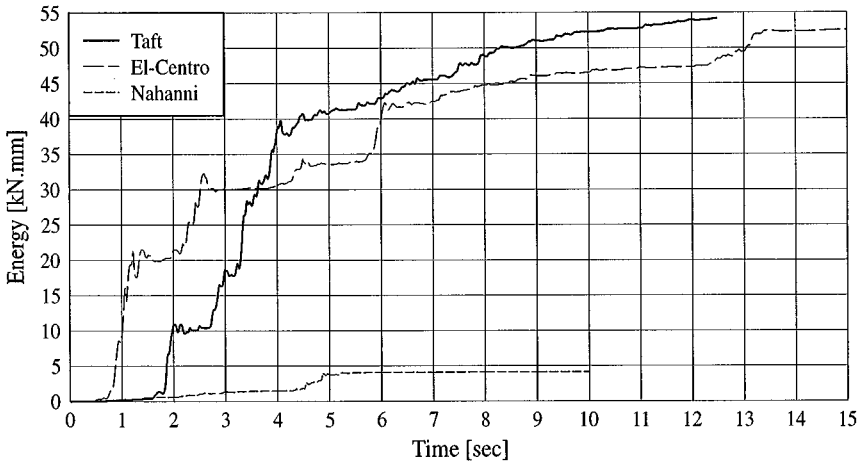

Figure 10. Imparted Energy for Taft, El-Centro and Nahanni earthquakes scaled to 0·075*g*

damping energy is nearly constant with increasing PGA. This is a direct consequence of using Rayleigh damping in the approximate numerical modeling of the viscous damping.

Based on the results given in Figure 12, the variation of the hysteretic energy (E_H) with the input energy (E_I) is illustrated in Figure 13. This figure implies an almost linear variation of E_H and E_I. From a previous study,[21] similar linear variation was observed from the results of quasi-static experi ments performed on single-storey structures similar to the two-storey structure tested in the present research.

5.3. Straining actions in the frame members

The time histories for the curvature at the indicated locations of the middle column of the first storey under the Taft earthquake scaled to 0·275*g* are shown in Figure 14. The corresponding bending moment diagram at the time of maximum base shear is shown in Figure 15. In this figure, the diagrams corresponding to both loading directions are shown and the maximum bending moments are indicated as a percentage of the yield moment M_y.[‖] The time histories for the normal forces in the locations of maximum bending moments are shown in Figure 16 for the Taft earthquake scaled to 0·275*g*.

Several relevant points may be made regarding the straining actions in the frame members. These are:

1. The bending moment diagram is significantly affected by the interaction between the infill walls and the bounding frame members.
2. Upon load reversal, the bending moment diagram is almost completely reversed even for highly damaged walls.

[‖] The yield moment is the nominal value of moment when the yield stress is reached at the extreme fibers of the section. For the steel section used in the columns (S 3 × 7·5), $M_y \approx 11{\cdot}0$ kN m.

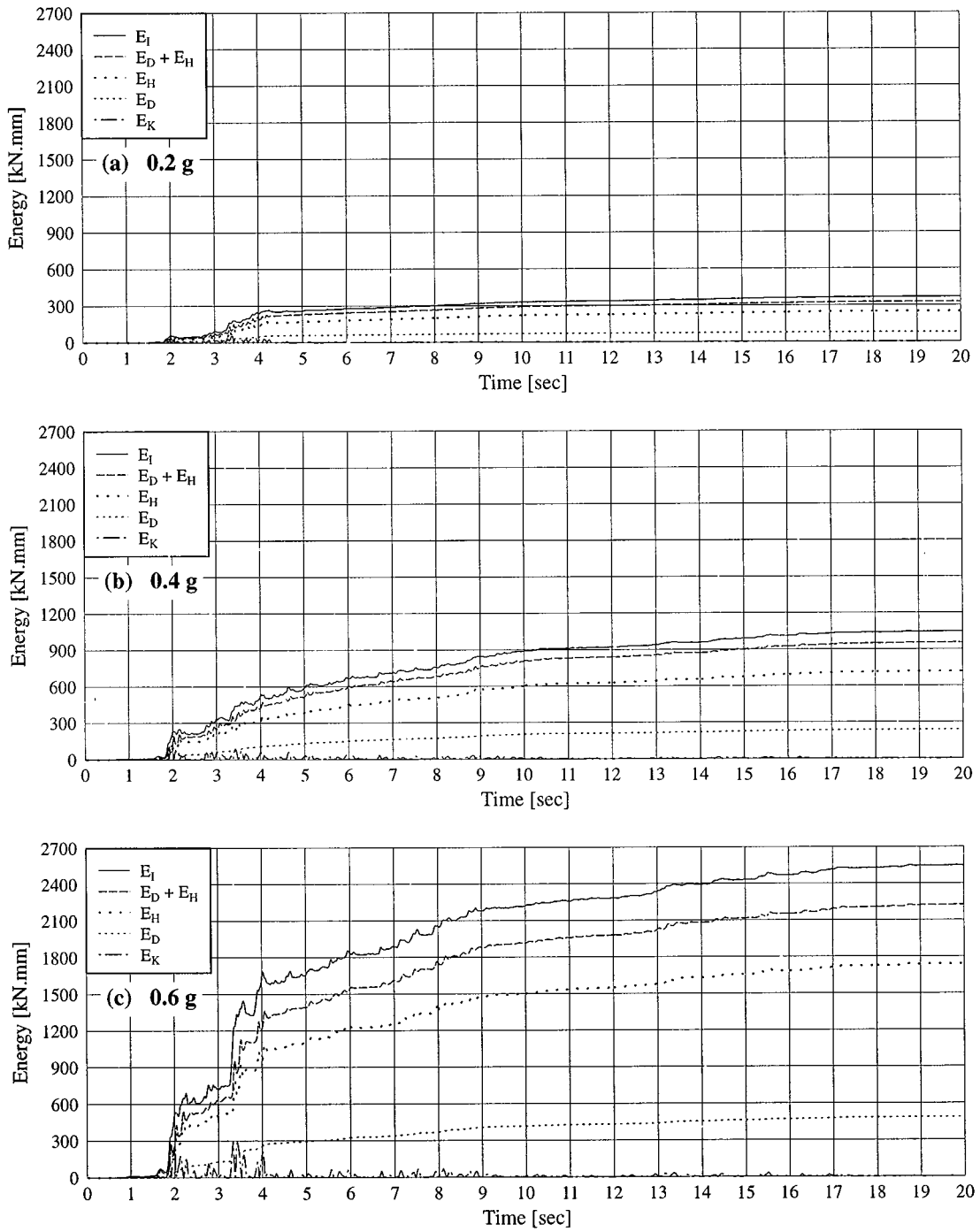

Figure 11. Time histories for energy terms under Taft earthquake

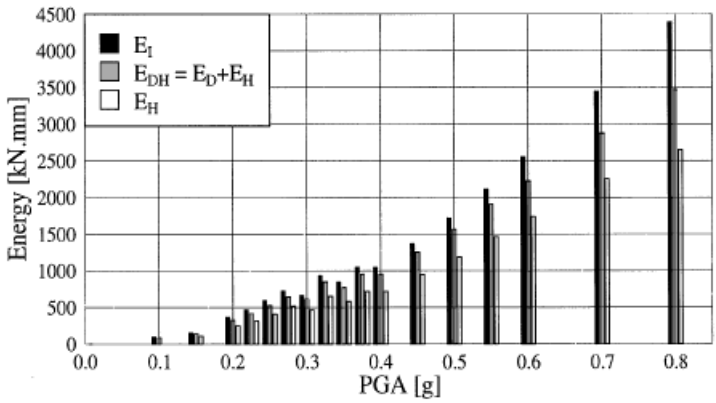

Figure 12. Variations of maximum values of energy terms with PGA

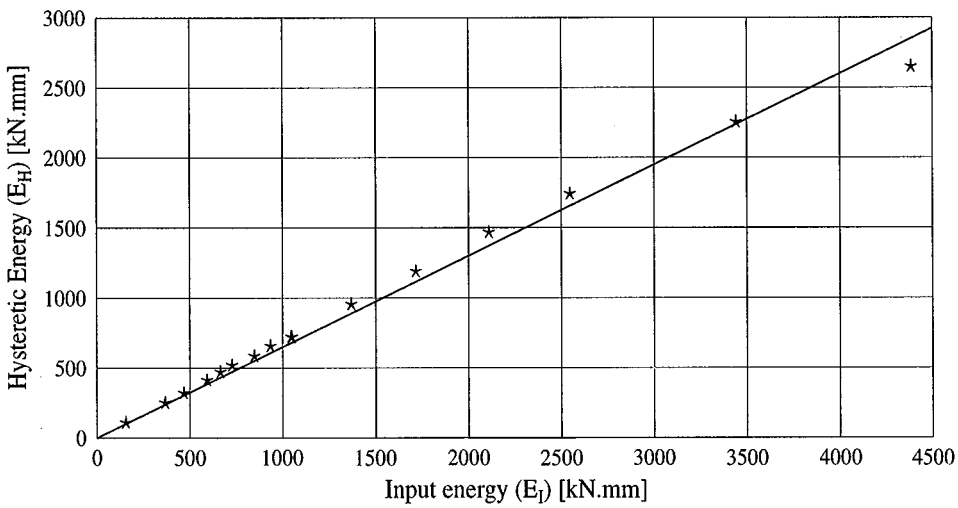

Figure 13. Variation of hysteretic energy with input energy

3. The section of the maximum bending moment is shifted away from the beam-to-column connections. This observation justifies the need for off-diagonal equivalent struts to properly account for the effect of infills on the internal forces of the frame members.**
4. The normal forces in the frame members are predominantly tension†† especially for intact walls.

** Reinforced concrete frames designed mainly for gravity loads without considering the infills have short splices in the longitudinal reinforcement of the columns. These splices are located just above the upper face of the beams. Accordingly, the observed shift in the location of the maximum bending moment may lead to serious effects on the performance of the reinforcing steel in the spliced region, i.e. high bond stress due to the insufficient development length.

†† For reinforced concrete frames, this observation has a strong impact on the cracking of the frame members when infills are included, especially if the gravity loads of upper stories are not considered in testing lower storey subassemblages.

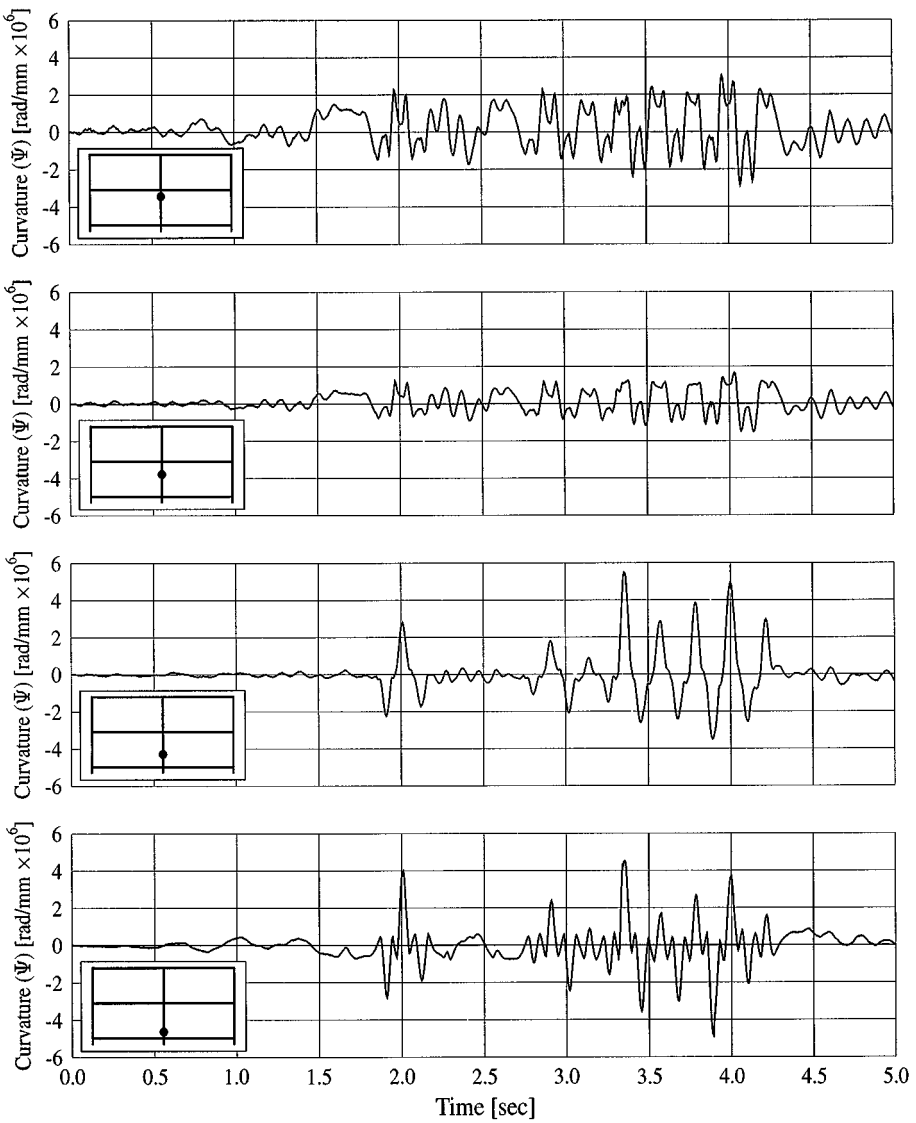

Figure 14. Time histories for the calculated curvatures along the middle column in the first storey under Taft earthquake scaled to 0·275*g*

5.4. Load path topology (equivalent truss model)

From the crack patterns obtained at PGA = 0·6*g* (Figure 9), an acceptable load path topology may be assumed a shown in Figure 17. This equivalent truss accounts for the expected compression and tension stress fields in the wall panels according to the loading direction. The material model of the compression struts should account for the capacity of *confined masonry* in axial compression. The tension members are necessary for equilibrium of the *bent* compression fields (struts) and they should be governed by the tensile behavior of cracked masonry. Typically, cracks in masonry zigzag through the bed and head mortar joints. Therefore, tensile behaviour of cracked masonry is governed by a combination of opening and sliding modes of these cracks.

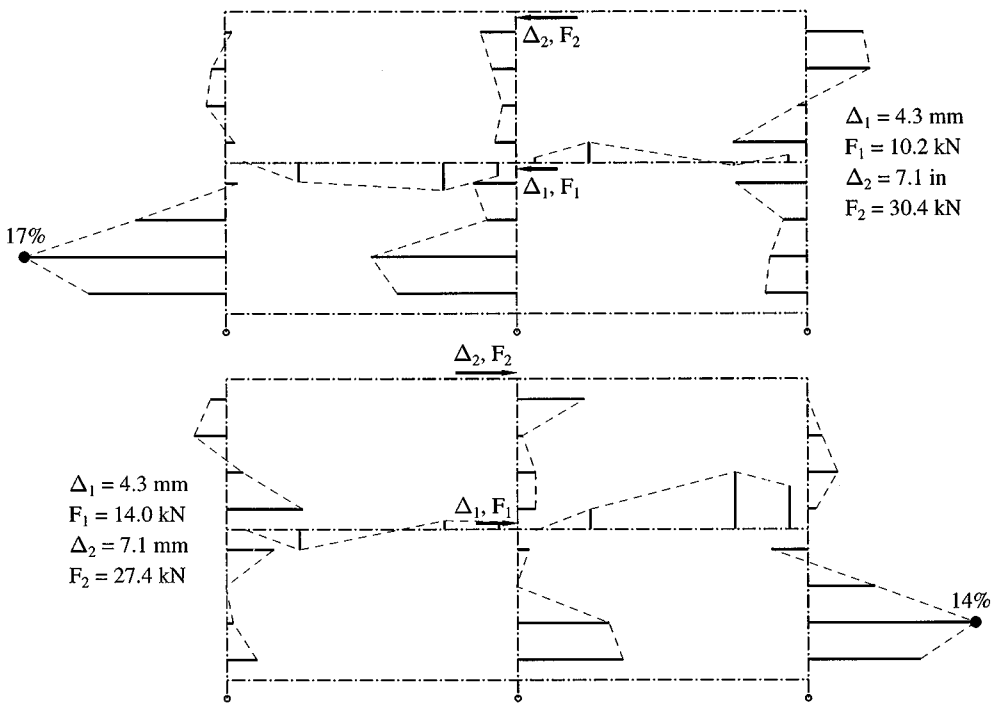

Figure 15. Bending moment diagram drawn in tension side at maximum base shear under Taft earthquake scaled to 0·275*g* (●: maximum value, given as per cent of M_y)

Each infill panel is modeled using two *independent* truss systems (i.e. dual system). At one instant, only one truss system is active. This may be achieved by adding a *gap element* at each nodal connection between the equivalent truss and the frame members as illustrated in Figure 17. The equivalent truss may be connected to the frame members at two or more points to consider *a priori* the finite *contact length* between the frame members and the infill walls. When the force across such a gap element becomes tensile, the associated truss members are deactivated. Based on the experimental observations, after cracking in the wall panels, significant *dilation* of such cracks produces wall/beam interaction. To account for this interaction, the beams may be connected to the equivalent truss through either compression-only vertical members or gap elements, depending on the topology of the truss, as shown in Figure 17.

6. CONCLUSIONS

The pseudo-dynamic experimentation technique and its analytical formulation is presented. Evaluation of the experimental errors and the numerical results of a simplified model substantiated the accuracy of the method. It is concluded that the implemented predictor–corrector algorithm allows excellent control over the experimental error propagation. The essentially static loading approach used in pseudo-dynamic testing permits careful documentation of the complex cracking and slipping behaviour of the infill walls, and the intricacies of the frame/wall interaction.

Results are presented from the pseudo-dynamic experiments performed on a two-bay, two-storey, gravity load designed steel frame with unreinforced concrete block masonry infill walls. The global response, in the form of crack patterns and correlation between hysteretic energy and imparted energy, of the infilled frame tested pseudo-dynamically was shown to be similar to observations from previous quasi-static experiments conducted on similar structures with single-storey. The discussion of the results shows the appropriateness of

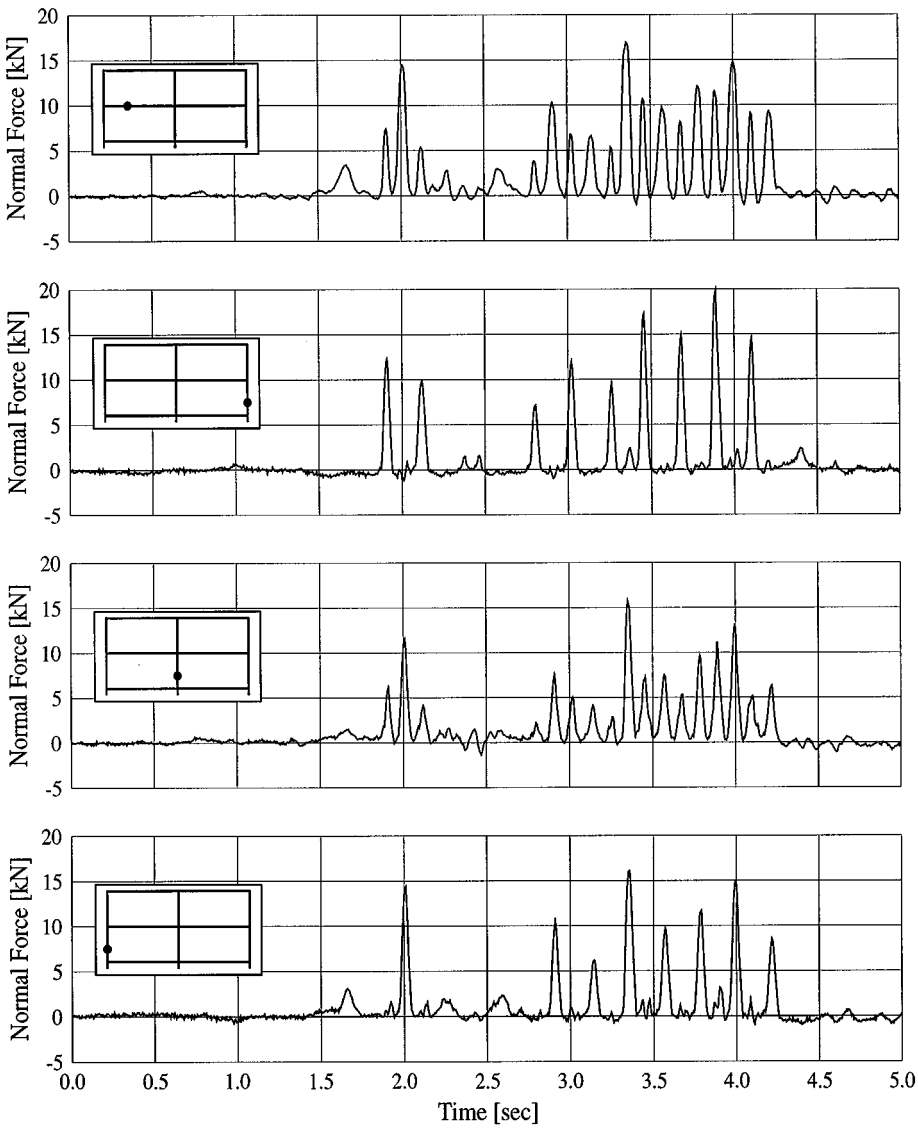

Figure 16. Time history for axial forces in frame members under Taft earthquake scaled to 0·275*g*

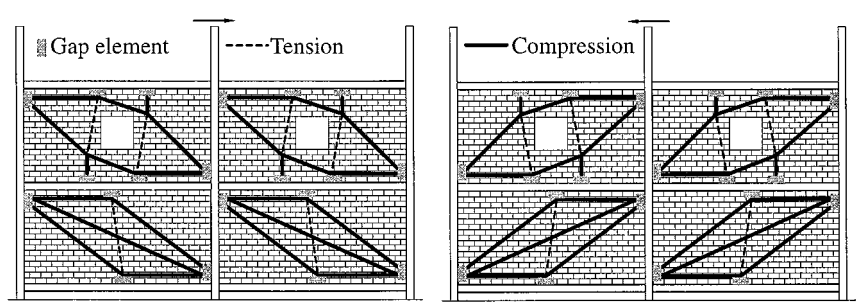

Figure 17. Loading paths in the infill walls based on the expected stress fields

the idealization of masonry infills as an equivalent dual truss system connected to the frame members through gap elements. Several energy terms are investigated. It is concluded that imparted energy and hysteretic energy correlate well with the observed damage state. Accordingly, variation of these terms with the increase of PGA may be considered as a global measure to quantify the damage state of the structure. Finally, the straining actions in the frame members are significantly affected by the presence of infills.

ACKNOWLEDGEMENTS

The financial support of the National Center for Earthquake Engineering Research (NCEER), with primary funding from the National Science Foundation and the State of New York, is gratefully acknowledged.

REFERENCES

1. J. L. Dawe and C. K. Seah, 'Behavior of masonry infill steel frames', *Canad. J. Civil Engng.* **16**, 865–876 (1989).
2. J. B. Mander, B. Nair, K. Wojtkowski and J. Ma, 'An experimental study on the seismic performance of brick-infilled steel frames with and without retrofit', *Technical Report NCEER-93-0001*, State University of New York at Buffalo (1993).
3. H. A. Moghaddam and P. J. Dowling, 'The state of the art in infilled frames', *ESEE Research Report No. 87-2*, Imperial College of Science and Technology, Civil Engng. Dept., London (1987).
4. K. Takanashi, K. Udagawa, M. Seki, T. Okada and H. Tanaka, 'Nonlinear earthquake response analysis of structures by a computer-actuator on-line system', *Bull. Earthquake Resist. Struct. Res. Center*, Tokyo **8** (1975).
5. K. Takanashi and M. Nakashima, 'Japanese activities on on-line testing', *J. Struct. Engng. ASCE* **113**, 7, 1014–1032 (1987).
6. P. B. Shing and S. A. Mahin, 'Pseudodynamic test method for seismic performance evaluation: Theory and implementation', *Report No. UCB/EERC-84/12*, Earthquake Engng. Res. Ctr., Univ. of California, Berkeley, 1984.
7. R. D. Hanson and N. H. McClamroch, 'Pseudo dynamic test method for inelastic building response', *Proc. 8th U.S. World Conf. Earthquake Engng.*, Vol. VI, San Francisco, California, 1984, pp. 127–134.
8. S. A. Mahin, P. B. Shing, C. R. Thewalt and R. D. Hanson, 'Pseudodynamic test method—current status and future directions', *J. Struct. Engng. ASCE* **115**, 2113–2128 (1989).
9. P. B. Shing and S. A. Mahin, 'Experimental error propagation in pseudodynamic testing', *Report No. UCB/EERC-83/12*, Earthquake Engng. Res. Ctr., Univ. of California, Berkeley, 1983.
10. C. R. Thewalt and S. A. Mahin, 'Hybrid solution techniques for generalized pseudodynamic testing', *Report No. UCB/EERC-87/09*, Earthquake Engng. Res. Ctr., Univ. of California, Berkeley, 1987.
11. P. B. Shing, M. T. Vannan and E. Carter, 'Implicit time integration for pseudodynamic tests', *Earthquake Engng. Struct. Dyn.* **20**, 551–576 (1991).
12. P. B. Shing, M. T. Vannan and E. Carter, 'Evaluation of reinforced masonry shear wall components by pseudodynamic testing', *Proc. 4th U.S. Natl. Conf. Earthquake Engng.*, Vol. II, Palm Springs, California, 1990, pp. 829–838.
13. P. B. Shing and S. A. Mahin, 'Cumulative experimental errors in pseudodynamic tests', *Earthquake Engng. Struct. Dyn.* **15**, 409–424 (1987).
14. P. B. Shing and S. A. Mahin, 'Experimental error effects in pseudodynamic tests', *J. Struct. Engng. ASCE* **116**, 4, 805–821 (1989).
15. Y. Yamazaki, M. Nakashima and T. Kaminosono, 'Reliability of pseudodynamic test in earthquake response simulation', *J. Struct. Engng. ASCE* **115**, 8, 2098–2112 (1989).
16. C. Thewalt and M. Roman, 'Performance parameters for pseudodynamic tests', *J. Struct. Engng. ASCE* **120**, 9, 2768–2781 (1994).
17. T. J. R. Hughes, 'Analysis of transient algorithms with particular reference to stability behavior', in *Mechanics and Mathematics Methods*: *A Series of Handbooks*, *First series*: *Computations Methods in Mechanics*, Vol. 1: *Computational Methods for Transient Analysis*, Chapter 2, T. Belytschko and T. J. R. Hughes (eds.), Elsevier, Amsterdam, 1983, pp. 67–156.
18. T. J. R. Hughes, K. S. Pister and R. L. Taylor, 'Implicit–explicit finite elements in nonlinear transient analysis', *Comput. Methods Appl. Mech. Engng.* **17**/**18**, 159–182 (1979).
19. G. M. Sabnis, H. G. Harris, R. N. White and M. S. Mirza, *Structural modeling and experimental techniques*, Prentice-Hall, Englewood Cliffs, NJ, 1983.
20. J. M. Biggs, *Introduction to Structural Dynamics*, McGraw-Hill, New York, 1964.
21. K. M. Mosalam, R. N. White and P. Gergely, 'Static response of infilled frames using quasi-static experimentation', *J. Struct. Engng. ASCE* **123**, 11, 1462–1469 (1997).
22. T. F. Zahrah and W. J. Hall, 'Earthquake energy absorption in SDOF structures', *J. Struct. Engng. ASCE* **110**, 8, 1757–1772 (1984).
23. C.-M. Uang and V. V. Bertero, 'Evaluation of seismic energy in structures', *Earthquake Engng. Struct. Dyn.* **19**, 77–90 (1990).

